Title: Single Cell Transcriptional Profiling of Phox2b-Expressing Geniculate Ganglion Neurons

Authors: Catherine B. Anderson and Eric D. Larson

Affiliations: Department of Otolaryngology, University of Colorado Anschutz Medical Campus, Aurora CO 80045

Article Type: Original Report

Author Roles: CBA performed experiments and analyzed data. EDL conceived and executed the study, performed analyses, and wrote the manuscript. All authors reviewed and approved the final manuscript.

Corresponding Author:

Eric D. Larson

University of Colorado, Department of Otolaryngology

12700 E. 19th Ave, MS 8606

Aurora, CO 80045

Key Words: Phox2b, geniculate ganglion, single cell sequencing, taste

Abstract

The sense of taste is fundamental for survival as harmful substances can be discriminated and prevented from entering the body. Taste buds act as chemosensory sentinels and detect bitter, salty, sweet, sour, and umami substances. Taste receptor cells within taste buds detect these sapid molecules and transmit signals to afferent nerve fibers. Whether a single gustatory nerve fiber selectively is responsive to a single taste modality (through taste receptor cell activation) is a point of contention in the field. Two studies have attempted to molecularly classify individual gustatory neurons using single cell RNA sequencing and two others have attempted to classify neurons based on physiological properties, with some conflicting results. In the present study, we present a method for single cell RNA sequencing of gustatory geniculate ganglion neurons and compare the results obtained to prior published works. We find multiple classes of ganglion neurons, but in conjunction with published works, the only clusters that can be clearly attributed to specific taste modalities are those involved in sweet or sour detection.

28 **Introduction:**

29 Taste buds detect sapid molecules in the mouth and are the initiators of gustation. Each taste bud
30 contains 50-100 taste receptor cells, which are classified as three separate types. Type I cells are the least
31 understood, but act as supporting cells and may transduce come portion of salty taste. Type II cells are well-
32 understood and transduce signals in response to bitter, sweet, or umami stimuli. Type II cells communicate
33 with afferent nerve fibers through release of ATP via non-traditional synaptic mechanisms(Finger et al., 2005;
34 Huang et al., 2007; Romanov et al., 2007, 2018; Taruno et al., 2013). Type III cells form classical synapses
35 with afferent nerve fibers and are responsible for sour and portions of salt taste detection. Due to the different
36 nature of how Type II and Type III cells communicate with afferent fibers, it is likely that the innervating fibers
37 have different molecular and physiological properties. Indeed, we have shown that afferent fibers that express
38 the serotonin receptor 5-HT3A preferentially contact serotonergic Type III cells (Stratford et al., 2017). This
39 subset of afferent fibers responds to exogenous serotonin as well as ATP while other gustatory fibers respond
40 only to ATP (Larson et al., 2015). These data suggest at least one subpopulation of gustatory afferent nerve
41 fibers.

42 Lingual taste fields are innervated by branches of the facial (cranial nerve VII) and glossopharyngeal
43 nerve (cranial nerve IX). The posterior tongue receives input from the lingual branch of the glossopharyngeal
44 nerve while the anterior tongue receives input from the chorda tympani branch of the facial nerve. The cell
45 bodies of the chorda tympani reside in the geniculate ganglion. In addition to the chorda tympani, this ganglion
46 houses the cell bodies of the greater superficial petrosal and the nervus intermedius which receive gustatory
47 input from the soft palate and somatosensory input from the external auditory meatus (Mtui et al., 2011).

48 We previously showed that the majority of geniculate ganglion neurons show excitatory responses to
49 exogenously applied ATP and about 25% to serotonin via P2X2/P2X3 and 5HT3A receptors, respectively
50 (Larson et al., 2015; Vandenbeuch et al., 2015). Older studies using patch clamp electrophysiology of rat
51 gustatory geniculate ganglion neurons also showed excitatory responses to ACh, serotonin, substance P, and
52 GABA in a small percentage of cells (King and Bradley, 2000; Koga and Bradley, 2000). These data suggest
53 that multiple classes of neurons exist at the physiological and that likely, these classes could be reflected at the
54 molecular level.

55 Gustatory geniculate ganglion neurons are delineated by expression of the transcription factor, *Phox2b*
56 (Dvoryanchikov et al., 2017; Ohman-Gault et al., 2017; Rios-Pilier and Krimm, 2019) which can molecular
57 define a neuron as gustatory or non-gustatory. The first study to characterize the transcriptome of single
58 geniculate ganglion neurons utilized the Fluidigm C1 to profile 96 neurons from wildtype mice (Dvoryanchikov
59 et al., 2017). They found about 2/3 of the cells express *Phox2b*, consistent with histological studies. Within the
60 gustatory cells, three main clusters were identified, all of which expressed *Phox2b* and *P2rx3*. Other cluster
61 markers included T1: *Olfm3*, *Itm2a*, *Hspb3*; T2: *Cd302*, *Kcnip1*, *Slc39a11*; T3: *Lypd1*, *Penk*, and *Trhr*. The
62 authors then characterized the physiological response profiles of isolated ganglion neurons to exogenous ATP
63 and 5-HT to match functional profiling with transcriptional profiling and demonstrated multiple physiological
64 profiles that nicely matched expression of P2X and 5-HT receptor mRNA. This study was the first to
65 characterize geniculate ganglion neurons at the molecular level using scRNA-seq.

More recently, Zhang et al. performed scRNA-sequence analysis on a larger cohort of geniculate ganglion neurons (Zhang et al., 2019). They profiled over 400 neurons using the Cel-seq (Hashimshony et al., 2012) method and identified 7 clusters. Based on cluster markers, they made multiple transgenic and knockout mice to test the role of certain transcripts in taste detection. Knockout of *Cdh4* and *Cdh13* eliminated detection of umami and bitter molecules, respectively, as assessed by two-bottle taste preference testing. Inhibition of *Egr2*-neurons using a *Egr2*-cre/Tetanus toxin model eliminated detection of NaCl. However, evidence for exactly how these transcripts are responsible for detecting taste modalities was not presented. However, more convincing evidence is presented for a class of sweet-best and sour-best neurons, marked by expression of *Spon1* and *Penk* transcripts, respectively. Using a floxed Gcamp model, the authors recorded in vivo calcium signals in geniculate ganglion neurons and showed that *Spon1* and *Penk* neurons selectively responded to sweet and sour lingual stimuli, respectively.

In the present study, we performed transcriptional profiling of geniculate ganglion neurons using an alternative method. We show that the neurons we collected expressed many transcripts overlapping with currently published datasets. Additionally, secondary analyses were performed on published datasets to further explore geniculate ganglion neuron clusters in attempt to understand more about the role of ganglion neurons in taste perception. Lastly, we show that combining all three datasets preserves cell clustering using the new analysis methods in Seurat V3.

Materials and Methods:

Animals

All animal procedures were conducted under a protocol approved by the University of Colorado Animal Care and Use Committee. Phox2bcre mice were purchased from Jax (B6(Cg)-Tg(Phox2b-cre)3Jke/J; stock # 016223) and bred to Rosa26/tdTomato mice (B6.Cg-Gt(ROSA)26Sortm14(CAG-tdTomato)Hze/J; stock # 007914). Crossed mice of both gender were used between the ages of 8 and 24 weeks.

Immunofluorescence

Animals were anesthetized using urethane and transcardially perfused with 4% paraformaldehyde in phosphate buffer (0.1M; PB) or euthanized with carbon dioxide. Geniculate ganglia and tongues were extracted and fixed for 1 or 4 hours at room temperature before incubating in 20% sucrose in PB overnight at 4C. Tissue was embedded and frozen in Optimal Cutting Temperature (OCT) and sectioned at a thickness of 12-16 um using a cryostat. After > 24 hours at -20C, slides were thawed, rehydrated with PBS, and blocked using 2% normal donkey serum in blocking buffer (PBS plus 0.3% TritonX100, 1% BSA). Primary antibodies were applied overnight at 4C. After thorough washing fluorescence secondary antibodies were applied at room temperature for 3 hours before counterstaining with DAPI and mounting with FluoroMountG (Southern Biotech). Slides were imaged using a Leica SP8 using 20x (NA 0.75) and 63x (NA 1.4) oil-immersion objectives.

Single cell preparation

104 Geniculate ganglia of three carbon dioxide-euthanized mice were rapidly extracted an placed in minimum
105 essential medium with Earle's balanced salts (MEM/EBSS; Hyclone) supplemented with 1.25 mg/ml trypsin
106 (Sigma-Aldrich) and 2.5 mg/ml collagenase A (Roche Diagnostics) for 30 minutes at 35C. Digested ganglia
107 were washed with MEM/EBSS, and gently triturated with a fire-polished glass pipette. The suspension was
108 passed through a 50 um filter and loaded as the top layer of a Percoll gradient (12.5 and 28%, Sigma-Aldrich;
109 Malin et al., 2007). The gradient was spun at 1300g for 10 minutes using a swinging bucket rotor. The cell
110 pellet at the bottom of the tube was washed with MEM/EBSS before resuspending in 2 mL MEM/EBSS.
111
112 *Single cell capture and RNA extraction*
113 A QiaScout Microraft Array (Qiagen) was coated with poly-D-lysine (0.02 mg/ml) for 2 hours and washed with
114 MEM/EBSS. The geniculate ganglion cell suspension was placed in the microraft array and the cells allowed to
115 settle for 20 minutes. The microraft array was secured using a custom set up to the stage of an Olympus IX71
116 inverted microscope equipped with a 10X objective and the QiaScout instrument (Qiagen). Cells were visually
117 inspected and microrafts containing a single tdTomato-positive (or negative in some cases) geniculate
118 ganglion neuron were extracted and transferred to a PCR tube containing lysis buffer as part of the QIAseq FX
119 Single Cell RNA Library Kit (Qiagen). Once in lysis buffer, cells were lysed by heating the tube to 95C for 3
120 minutes followed by an infinite hold at 4C until 24 individual samples were collected. The collection protocol
121 was performed across two independent experiments, resulting in 48 individual sequencing libraries (42
122 tdTomato+, 6 tdTomato-).
123
124 *Library preparation and sequencing*
125 Sequencing libraries were prepared using the QIAseq FX Single Cell RNA Library Kit (Qiagen) according to
126 manufacturer instructions. Cells were lysed, followed by gDNA removal, reverse transcription, ligation, and
127 whole transcriptome amplification. After amplification, libraries were enzymatically fragmented (~300 bp
128 fragments) followed by adapter ligation. Library size was evaluated using a DNA tapestation and concentration
129 was determined using qPCR (QIAseq Library Quant Array). Libraries were pooled at equimolar concentration
130 and sequenced using an Illumina MiSEQ to generate 2x151 bp reads.
131
132 *Sequencing analysis*
133 Quality and adapter trimming was performed using BBDuk (Bushnell). Salmon (v0.14.0) was used to quantify
134 transcript expression using trimmed reads and the Ensembl GRCm38.p6 (version 92) transcriptome (Patro et
135 al., 2017; Zerbino et al., 2018). Transcript expression was summarized at the gene level and input to R using
136 TxImport (Soneson et al., 2016; R Core Team, 2019). A custom R script was used to visualize gene
137 expression in the dataset. Samples were kept if expression of *Snap25* or *Uclh1* was > 5 TPM. Discarded
138 samples were further interrogated for expression of neuron-specific genes, but they were rarely present.
139
140 *Sequencing analysis of published datasets*

141 Single cell sequencing FASTQ files were obtained from NCBI Gene Expression Omnibus (GSE102443
142 (Dvoryanchikov et al., 2017) and GSE135801 (Zhang et al., 2019)). Raw reads from Dvoryanchikov et al. were
143 filtered, trimmed, mapped, and summarized at the gene-level using the same tools as described above. A
144 processed gene count matrix was obtained from Zhang et al. Gene count matrices were used as the input for
145 Seurat (V3; ref) where samples were filtered, scaled, and clustered.
146
147 *Meta analysis of datasets*
148 Individual Seurat objects were read in to R and processed using Seurat following the "Multiple Dataset
149 Integration and Label Transfer" vignette available on the program website
150 (https://satijalab.org/seurat/v3.1/integration.html).
151
152 *Data visualization*
153 Data were visualized using the pheatmap package in R or with Seurat plotting features DimPlot and
154 DoHeatmap and FeaturePlot (Butler et al., 2018; Kolde, 2019; Stuart et al., 2019).
155
156 **Results:**
157 *Characterization of Phox2b-cre mouse*
158 To confirm that the *Phox2b*-cre driver faithfully drives CRE recombinase in PHOX2B-expressing cells,
159 geniculate ganglia and gustatory taste fields of *Phox2b*-cre/Rosa-tomato mice were examined using confocal
160 immunofluorescence microscopy. A subset of geniculate ganglion neurons expresses robust tdTomato
161 fluorescence consistent with previous reports(Ohman-Gault et al., 2017; Rios-Pilier and Krimm, 2019). The
162 majority of tdTomato-expressing neurons exhibited P2X3 immunoreactivity, and conversely, nearly all P2X3-
163 immunoreactive neurons exhibited tdTomato fluorescence (Figure 1). To confirm that tdTomato is being driven
164 in PHOX2B-expressing ganglion cells, sections were labeled with an antibody against PHOX2B. Indeed, every
165 tdTomato-expressing neuron showed positive nuclear labeling of the transcription factor (Figure 1).
166 Within taste papillae, tdTomato positive nerve fibers enter taste buds consistent with the *Phox2b* as a
167 marker of gustatory nerve fibers. Most tdTomato-expressing nerve fibers exhibit strong P2X3-immunoreactivity.
168 Additionally, these fibers are rarely outside of taste buds but when present are not immunoreactive for P2X3
169 (Figure 2)
170
171 *scRNA-seq of Phox2b geniculate ganglion neurons*
172 To understand how gustatory nerve fibers communicate with taste receptor cells, single cell RNA sequencing
173 was performed on manually isolated geniculate ganglion neurons (48 samples from 6 total mice across 2
174 collection days; 40 tdTomato+, 6 tdTomato-, 2 blanks). Ganglion neurons were enzymatically digested and
175 plated on a Qiagen QiaScout Microraft array. Using the QiaScout device cells were visually inspected for
176 presence or absence of tdTomato, dislodged from the microraft array, and transferred to cell lysis buffer where
177 lysis was initiated followed by reverse transcription, whole transcriptome amplification, and sequencing library

178 preparation. Post processing of the sequencing data excluded samples that had < 50% mapping rate,
179 expression of *Snap25* or *Uchl1* < 5 TPM, and >2000 unique genes resulted in 31 cells (17 tdTomato+, 4
180 tdTomato-). *Phox2b* expression correlated with tdTomato fluorescence (Figure 3) and taste-related transcripts
181 (*P2rx2, P2rx3*) were present in all *Phox2b*+ neurons. A subset of *Phox2b*+ neurons also expressed *Htr3a*
182 (Figure 3). Additionally, genes such as *Penk and Spon1*, markers of sour-best and sweet-best neurons (Zhang
183 2019) were identified in some neurons. Unfortunately, the low sample size prevented use of unbiased
184 clustering algorithms such as Seurat (Stuart et al., 2019).
185
186 *Analysis of other datasets*
187 Zhang et al 2019 manually collected over 800 *P2rx3*-tdTomato expressing geniculate ganglion cells and
188 performed scRNA-sequencing using the Cel-seq technology. Of the 454 neurons available from GEO:
189 GSE135801, 258 had expression of >4000 unique genes. Zhang et al reported identifying clusters enriched for
190 *Spon1, Penk, Cdh4, Cdh13, and Egr2* and showed that neurons from those classes were selective for sweet,
191 sour, umami, bitter, and salty taste modalities, respectively. Analysis of raw RPM from these cells shows
192 similar patters to the data in this paper including expression of *P2rx3, P2rx3, Phox2b, Gabra1, Penk, Spon1,*
193 *and Htr3a* (Figure 4A). Seurat cluster analysis reveals 7 molecularly distinct neuronal clusters including those
194 marked by *Spon1* (cluster 2), *Penk* (cluster 3), *Cdh13* (clusters 1 and 5), and *Piezo2* (clusters 0 and 6; Figure
195 4B,C). However, *Cdh4* and *Egr2* were not detected as significant markers. The top 5 cluster makers (FDR-
196 pvalue <0.001, weighted by log fold change) for each cluster are plotted in Figure 4D. All cluster markers can
197 be found in Table S1.
198
199 An earlier report used wildtype mice and the Fluidigm C1 platform to perform expression profiling and
200 demonstrated 4 cell clusters (3 gustatory, 1 non-gustatory). Analysis of 96 cells using Seurat reveals 6 clusters
201 of cells (Figure 5B). The discrepancy among cluster numbers likely arises due to 1) different clustering
202 software/algorithms and 2) less conservative clustering variables. Indeed, the cluster identified by expression
203 of *Olfm3* in the original report was subdivided to three clusters in this current analysis (clusters 1,3,5). About
204 60% of profiled cells were gustatory based on expression of *Phox2b*. Consistent with Zhang et al 2019, *Penk*
205 (cluster 2), *Spon1* (cluster 5), *Piezo2* (clusters 0 and 4), and *Cdh13* (clusters 1 and 3) were significant clusters
206 identifiers (Figure 5C, D). Similar to above, neither *Egr2* nor *Cdh4* were identified as cluster markers. All cluster
207 markers can be found in Table S2.
208
209 *Meta analysis of all datasets*
210 Generally, in RNA-sequence analysis, it is against best-practices to combine datasets from multiple sources
211 given the range of variability in sample preparation, sequencing, and data processing. However, with recent
212 the release of Seurat V3 a method for combining datasets from single cell sequencing experiments across
213 multiple technologies has been developed (Stuart et al., 2019). This method finds integration anchors common

214 amongst the datasets, merges the data, and scales the data based on the anchors. This meta analysis allows
215 for integration of data on similar cell types from multiple sources.
216 The three datasets in this paper can be combined, scaled, and clustered together. Interestingly, UMAP
217 plotting of the integrated data shows a strong similarly among three datasets, with cells from each dataset
218 being represented throughout the plot (Figure 6A,B). This suggests that despite three different methods and
219 technologies used to collect scRNA-seq data, the genetic information was similar between studies. Clustering
220 of the integrated data reveals 7 cell clusters. *Penk* (cluster 3), *Spon1* (cluster 4), *Piezo2* (clusters 0 and 6), and
221 *Cdh13* (clusters 5), *Egr2* (cluster 2), and *Cdh4* (cluster 2) were significant cluster identifiers (Figures C,D). All
222 cluster markers can be found in Table S3.
223
224 **Discussion:**
225 *Do neuron clusters represent specific taste modalities?*
226 Single cell RNA-seq allows for the determination of heterogeneity within a cell population. By clustering
227 cells based on similarities, markers that are unique to those clusters can be identified, which can give strong
228 insight to their function. While Dvoryanchikov et al. were the first reveal molecular heterogeneity by identifying
229 clusters of geniculate ganglion neurons, Zhang et al. were the first to attribute the role of specific cell clusters
230 to taste detection. Convincing evidence demonstrates that neurons in the *Penk* and *Spon1*- expressing cell
231 clusters represent sour- and sweet-best neurons. Thus, it is plausible that these neurons receive specific input
232 from Type III and Type II taste receptor cells, respectively.
233 Sour and sweet: All three datasets analyzed in the present study showed expression of *Penk* and
234 *Spon1* in gustatory fibers and that they marked specific cell clusters. In Zhang et al 2019, *Penk* and *Spon1*
235 were cluster markers. Dvoryanchikov et al 2017 reported *Penk* as a cluster marker, but not *Spon1*.
236 Interestingly, secondary analysis reveals that *Spon1* neurons were a subset of the cluster labeled 'T1' in the
237 original report, which was subdivided in to three clusters in this current study (Figure 5C). These findings
238 together with the in vivo imaging of Zhang et al 2019 strongly suggest that sour-best and sweet-best fibers are
239 molecularly distinct from other ganglion neurons.
240 Bitter, salty, and umami: Zhang et al reports that *Cdh4*, *Egr2*, and *Cdh13* are cluster markers for bitter,
241 salty, and umami-best neurons. However, in the present analyses, these markers did not clearly define clusters
242 as well as *Penk* and *Spon1*. Additionally, the behavioral assays performed by Zhang et al relied on constitutive
243 knockout of *Cdh4* and *Cdh13* and tetanus toxin inactivation of *Egr2* neurons. While the experiments showed
244 that umami, bitter, and salty taste preference rely on these transcripts, they do not show that this requirement
245 is at the level of the geniculate ganglion. Indeed, according to the Allen Brain Map, these three transcripts are
246 expressed in a variety of cell types throughout the central nervous system. Additionally, according to
247 secondary analysis of Qin et al, *Cdh13* is expressed in both Type II and Type III taste receptor cells and *Egr2*
248 is expressed in some Type III cells (not shown; Qin et al., 2018). Thus, any ganglion cell clusters responsible
249 for the detection of bitter, salty, and umami signals from taste receptor cells remains enigmatic.
250
251 *Does Htr3a mark a specific cluster?*

We previously showed that nerve fibers expressing the serotonin receptor 5-HT3 preferentially contact Type III taste receptor cells in all taste fields (Stratford et al 2017) suggesting that these fibers may be molecularly distinct within the geniculate ganglion. However, Dvoryanchikov et al. argued that *Htr3a* did not delineate a specific cluster in their analyses. In the present analyses, all three datasets show clustering of *Htr3a*-expressing neurons. While *Htr3a* was in multiple clusters, it had strongest expression in the cluster marked by *Penk* – the sour-best fibers which support our findings that these cells wire to sour-sensing Type III taste receptor cells. Conversely, *Htr3a* is absent in the *Spon1* cluster (sweet-best fibers). Interestingly, in all datasets, *Htr3a* is also present in a gustatory (*Phox2b*+) cluster expressing *Piezo2*, a transcript for a mechanosensitive channel. This cluster expressed low levels of *P2rx3*, and no *P2rx2*. Moayedi et al showed that *Piezo2*-GFP expressing nerve fibers are present in fungiform papillae, just adjacent to taste buds, and that these fibers enter the papillae in a bundle with other gustatory fibers (Moayedi et al., 2018). Interestingly, P2X2/3 double knockout mice (which lack nerve response to all tastants) still show nerve responses to mechanical stimulation of the tongue (Finger et al., 2005). Perhaps this *Piezo2*/*Htr3a*/*Phox2b* neuronal cluster is responsible for this ATP-independent response.

Conclusions

Overall, the data analyzed in this paper suggest molecular heterogeneity among the neurons of the geniculate ganglion. The datasets clearly separate gustatory vs non-gustatory neurons by expression of *Phox2b*. Within the *Phox2b* expressing fibers, clear sub clusters are formed. Consistent among the datasets are clusters defined by *Penk*, *Spon1*, and *Piezo2*. Zhang et al showed that *Penk* clusters represent sour-best fibers while *Spon1* clusters represent sweet-best fibers. The *Piezo2* cluster could be responsible for mechanosensation of the fungiform papillae. The remaining clusters were more variable between the datasets and markers identified by Zhang et al (*Cdh4*, *Cdh13*, *Egr2*) were not clearly observed in this study. While it is likely that neurons responsible for detecting each taste modality are molecularly distinct, more work needs to be done to elucidate the molecular phenotypes of bitter, salty, and umami sensitive fibers.

Figure Legends:

Figure 1. tdTomato expression in PHOX2B-immunoreactive neurons. Sections of Phox2bcre/tdTomato geniculate ganglion labeled with antibodies against PHOX2B and P2X3. Nearly all tdTomato-expressing cells are immunoreactive for PHOX2B and P2X3. Non-nuclear “green” signal is due to binding of anti-mouse secondary antibodies to endogenous mouse IgG; this signal persists in no primary controls ,and no nuclear signal is observed. Sections are maximal z-projections of ~12 μm image stacks.

Figure 2. tdTomato-expressing nerve fibers enter taste buds. Sections of lingual taste papillae showing immunoreactivity to GNAT3 (α-gustducin; Type II cells) and P2X3 with endogenous tdTomato fluorescence. Within taste buds, all tdTomato+ fibers exhibit P2X3 immunoreactivity. In some cases, tdTomato+ fibers were found in the intergemmal area and were P2X3 negative. Images are maximal z-projections of ~12-16 μm image stacks.

290

291 Figure 3. Expression of select transcripts in tdTomato-expressing neurons. Geniculate ganglion neurons were
292 collected using the QiaScout and processed for single cell RNA sequencing using the Qiagen FX single cell
293 RNA kit. Heatmap shows log(transcripts per million) of select transcripts. *Phox2b* expression correlates with
294 presence or absence of tdTomato.

295

296 Figure 4. Secondary analysis of Zhang et al. 2019 scRNA-seq data. Analysis of cells publicly available from
297 GSE135801. A. Heatmap showing log(reads per million) of select transcripts across all cells. B. Seurat UMAP
298 clustering of cells expressing greater than 2000 genes. C. Heatmap showing transcript expression of same
299 genes as in A, but after scaling and clustering in Seurat. D. Heatmap showing transcript expression of top 5
300 markers of each cluster. Clusters in C and D correlate with clusters in B.

301

302 Figure 5. Secondary analysis of Dvoryanchikov et al. 2017 scRNA-seq data. Analysis of cells publicly available
303 from GSE102443. Raw FASTQ files were analyzed to quantify transcript expression. A. Heatmap showing
304 log(reads per million) of select transcripts across all cells. B. Seurat UMAP clustering of cells expressing
305 greater than 2000 genes. C. Heatmap showing transcript expression of same genes as in A, but after scaling
306 and clustering in Seurat. D. Heatmap showing transcript expression of top 5 markers of each cluster. Clusters
307 in C and D correlate with clusters in B.

308

309 Figure 6. Combination of data from this paper, Dvoryanchikov et al 2017, and Zhang et al 2019. A. Seurat
310 UMAP clustering showing each dataset. Each cluster has cells from each dataset, though some cluster lack
311 cells from 'this study' likely due to the small sample size. B. Overall clusters of the combined datasets. C.
312 Heatmap showing transcript expression of select genes after scaling and clustering in Seurat. D. Heatmap
313 showing transcript expression of top 5 markers of each cluster. Clusters in C and D correlate with clusters in B.
314 E. Gene expression overlay of UMAP cluster plot shows expression of each gene. Each point represents a
315 single cell.

316

317 Table S1. Seurat-identified cluster markers for Zhang et al 2018.

318

319 Table S2. Seurat-identified cluster markers for Dvoryanchikov et al 2017.

320

321 Table S3. Seurat-identified cluster markers for meta analysis.

322

323 **Conflict of Interest:**

324 The authors have no financial conflicts of interest to declare.

325

326 **Funding:**

This work was supported by NIH/NIDCD R21DC015115-01 to Sue C. Kinnamon (University of Colorado Anschutz Medical Campus).

Acknowledgments:

We thank Qiagen for allowing us to demo the QiaScout device and supplying samples of the QiaScout Microraft Arrays.

335 **References:**

336 Bushnell, B. BBMap.

337 Butler, A., Hoffman, P., Smibert, P., Papalexi, E., and Satija, R. 2018. Integrating single-cell transcriptomic
338 data across different conditions, technologies, and species. Nature Biotechnology. 36:411–420.

339 Dvoryanchikov, G., Hernandez, D., Roebber, J.K., Hill, D.L., Roper, S.D., and Chaudhari, N. 2017.
340 Transcriptomes and neurotransmitter profiles of classes of gustatory and somatosensory neurons in the
341 geniculate ganglion. Nature Communications. 8:760.

342 Finger, T.E., Danilova, V., Barrows, J., Bartel, D.L., Vigers, A.J., Stone, L., Hellekant, G., and Kinnamon, S.C.
343 2005. ATP Signaling Is Crucial for Communication from Taste Buds to Gustatory Nerves. Science. 310:1495–
344 1499.

345 Hashimshony, T., Wagner, F., Sher, N., and Yanai, I. 2012. CEL-Seq: Single-Cell RNA-Seq by Multiplexed
346 Linear Amplification. Cell Reports. 2:666–673.

347 Huang, Y.-J., Maruyama, Y., Dvoryanchikov, G., Pereira, E., Chaudhari, N., and Roper, S.D. 2007. The role of
348 pannexin 1 hemichannels in ATP release and cell–cell communication in mouse taste buds. PNAS. 104:6436–
349 6441.

350 King, M.S., and Bradley, R.M. 2000. Biophysical properties and responses to glutamate receptor agonists of
351 identified subpopulations of rat geniculate ganglion neurons. Brain Research. 866:237–246.

352 Koga, T., and Bradley, R.M. 2000. Biophysical Properties and Responses to Neurotransmitters of Petrosal and
353 Geniculate Ganglion Neurons Innervating the Tongue. J Neurophysiol. 84:1404–1413.

354 Kolde, R. 2019. pheatmap: Pretty Heatmaps.

355 Larson, E.D., Vandenbeuch, A., Voigt, A., Meyerhof, W., Kinnamon, S.C., and Finger, T.E. 2015. The Role of
356 5-HT3 Receptors in Signaling from Taste Buds to Nerves. J Neurosci. 35:15984–15995.

357 Malin, S.A., Davis, B.M., and Molliver, D.C. 2007. Production of dissociated sensory neuron cultures and
358 considerations for their use in studying neuronal function and plasticity. Nat Protocols. 2:152–160.

359 Moayedi, Y., Duenas-Bianchi, L.F., and Lumpkin, E.A. 2018. Somatosensory innervation of the oral mucosa of
360 adult and aging mice. Sci Rep. 8:1–14.

361 Mtui, E., Gruener, G., and FitzGerald, M. 2011. Clinical Neuroanatomy and Neuroscience - 6th Edition.

362 Ohman-Gault, L., Huang, T., and Krimm, R. 2017. The transcription factor Phox2b distinguishes between oral
363 and non-oral sensory neurons in the geniculate ganglion. J Comp Neurol. 525:3935–3950.

364 Patro, R., Duggal, G., Love, M.I., Irizarry, R.A., and Kingsford, C. 2017. Salmon: fast and bias-aware
365 quantification of transcript expression using dual-phase inference. Nat Methods. 14:417–419.

366 Qin, Y., Sukumaran, S.K., Jyotaki, M., Redding, K., Jiang, P., and Margolskee, R.F. 2018. Gli3 is a negative
367 regulator of Tas1r3-expressing taste cells. PLOS Genetics. 14:e1007058.

368 R Core Team. 2019. R: A Language and Environment for Statistical Computing. Vienna, Austria: R Foundation
369 for Statistical Computing.

370 Rios-Pilier, J., and Krimm, R.F. 2019. TrkB expression and dependence divides gustatory neurons into three
371 subpopulations. Neural Dev. 14:3.

372 Romanov, R.A., Lasher, R.S., High, B., Savidge, L.E., Lawson, A., Rogachevskaja, O.A., Zhao, H.,
373 Rogachevsky, V.V., Bystrova, M.F., Churbanov, G.D., et al. 2018. Chemical synapses without synaptic

374 vesicles: Purinergic neurotransmission through a CALHM1 channel-mitochondrial signaling complex. Sci
375 Signal. 11:eaao1815.

376 Romanov, R.A., Rogachevskaja, O.A., Bystrova, M.F., Jiang, P., Margolskee, R.F., and Kolesnikov, S.S. 2007.
377 Afferent neurotransmission mediated by hemichannels in mammalian taste cells. The EMBO Journal. 26:657–
378 667.

379 Soneson, C., Love, M.I., and Robinson, M.D. 2016. Differential analyses for RNA-seq: transcript-level
380 estimates improve gene-level inferences. F1000Res. 4.

381 Stratford, J., Larson, E., Yang, R., Salcedo, E., and Finger, T. 2017. 5-HT3a-driven GFP delineates Gustatory
382 Fibers innervating Sour-responsive Taste Cells: A Labeled Line for Sour Taste? J Comp Neurol. 525:2358–
383 2375.

384 Stuart, T., Butler, A., Hoffman, P., Hafemeister, C., Papalexi, E., Mauck, W.M., Hao, Y., Stoeckius, M.,
385 Smibert, P., and Satija, R. 2019. Comprehensive Integration of Single-Cell Data. Cell. 177:1888-1902.e21.

386 Taruno, A., Vingtdeux, V., Ohmoto, M., Ma, Z., Dvoryanchikov, G., Li, A., Adrien, L., Zhao, H., Leung, S.,
387 Abernethy, M., et al. 2013. CALHM1 ion channel mediates purinergic neurotransmission of sweet, bitter and
388 umami tastes. Nature. 495:223–226.

389 Vandenbeuch, A., Larson, E.D., Anderson, C.B., Smith, S.A., Ford, A.P., Finger, T.E., and Kinnamon, S.C.
390 2015. Postsynaptic P2X3-containing receptors in gustatory nerve fibres mediate responses to all taste qualities
391 in mice. J Physiol. 593:1113–1125.

392 Zerbino, D.R., Achuthan, P., Akanni, W., Amode, M.R., Barrell, D., Bhai, J., Billis, K., Cummins, C., Gall, A.,
393 Girón, C.G., et al. 2018. Ensembl 2018. Nucleic Acids Res. 46:D754–D761.

394 Zhang, J., Jin, H., Zhang, W., Ding, C., O'Keeffe, S., Ye, M., and Zuker, C.S. 2019. Sour Sensing from the
395 Tongue to the Brain. Cell.

396

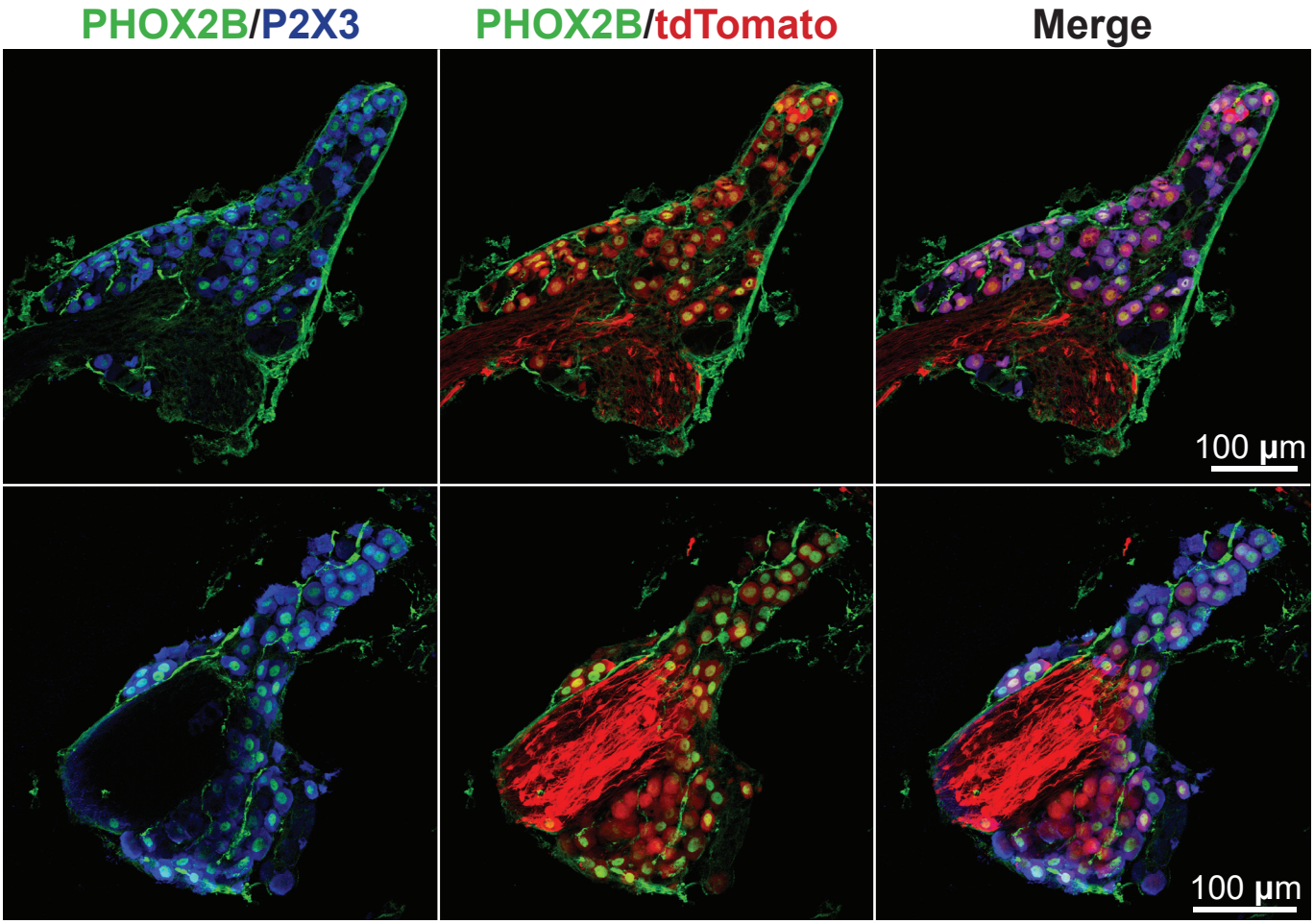

Figure 1

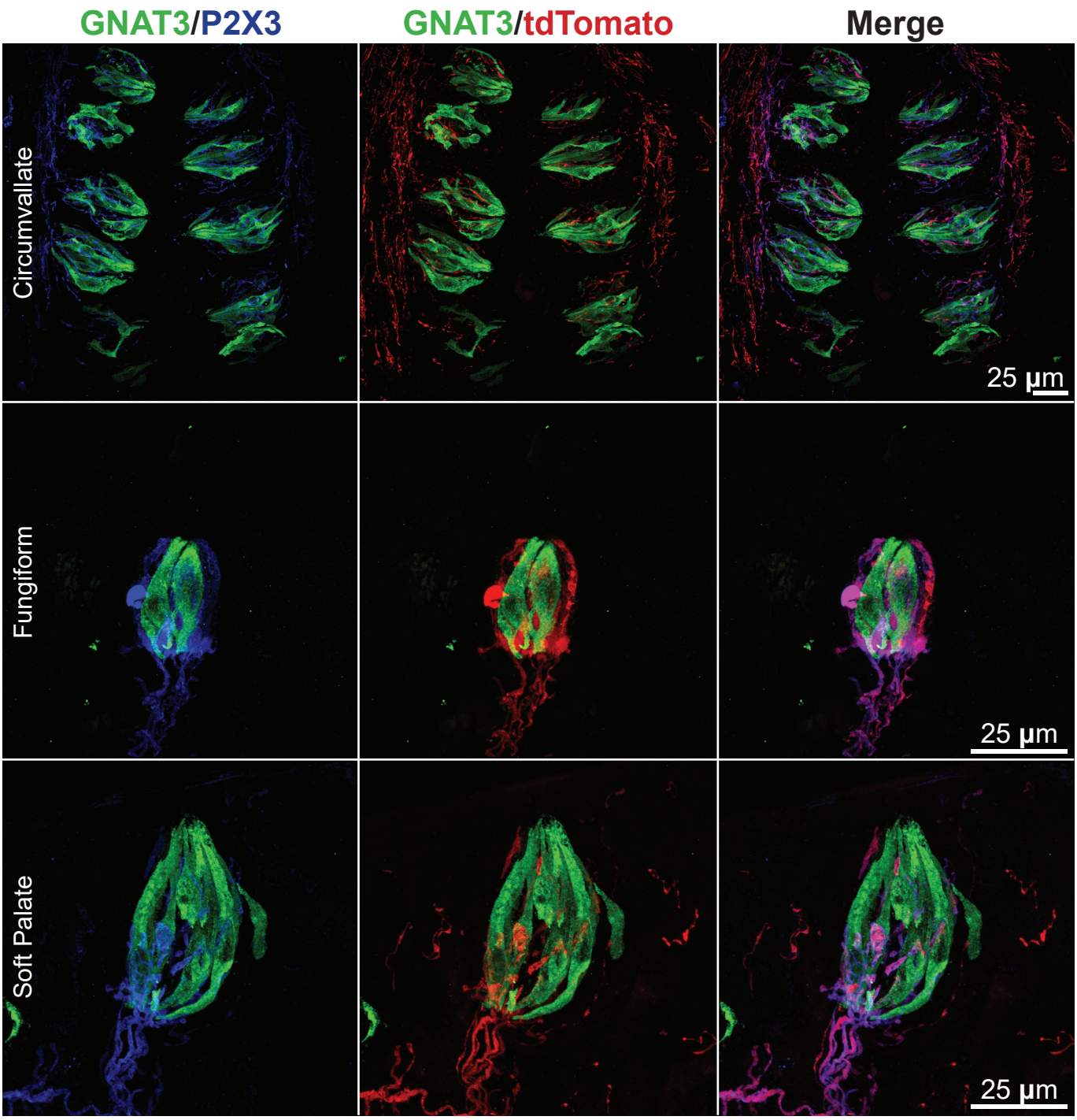
GNAT3/P2X3
GNAT3/tdTomato
Merge
Circumvallate
Fungiform
Soft Palate
25 µm
25 µm
25 µm

Figure 2

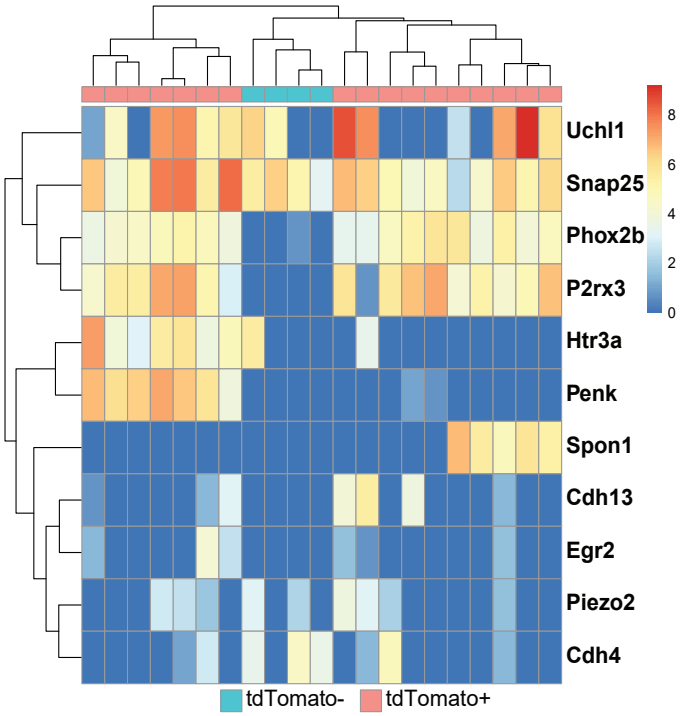
Uchl1
Snap25
Phox2b
P2rx3
Htr3a
Penk
Spon1
Cdh13
Egr2
Piezo2
Cdh4
8
6
4
2
0
tdTomato-
tdTomato+

Figure 3

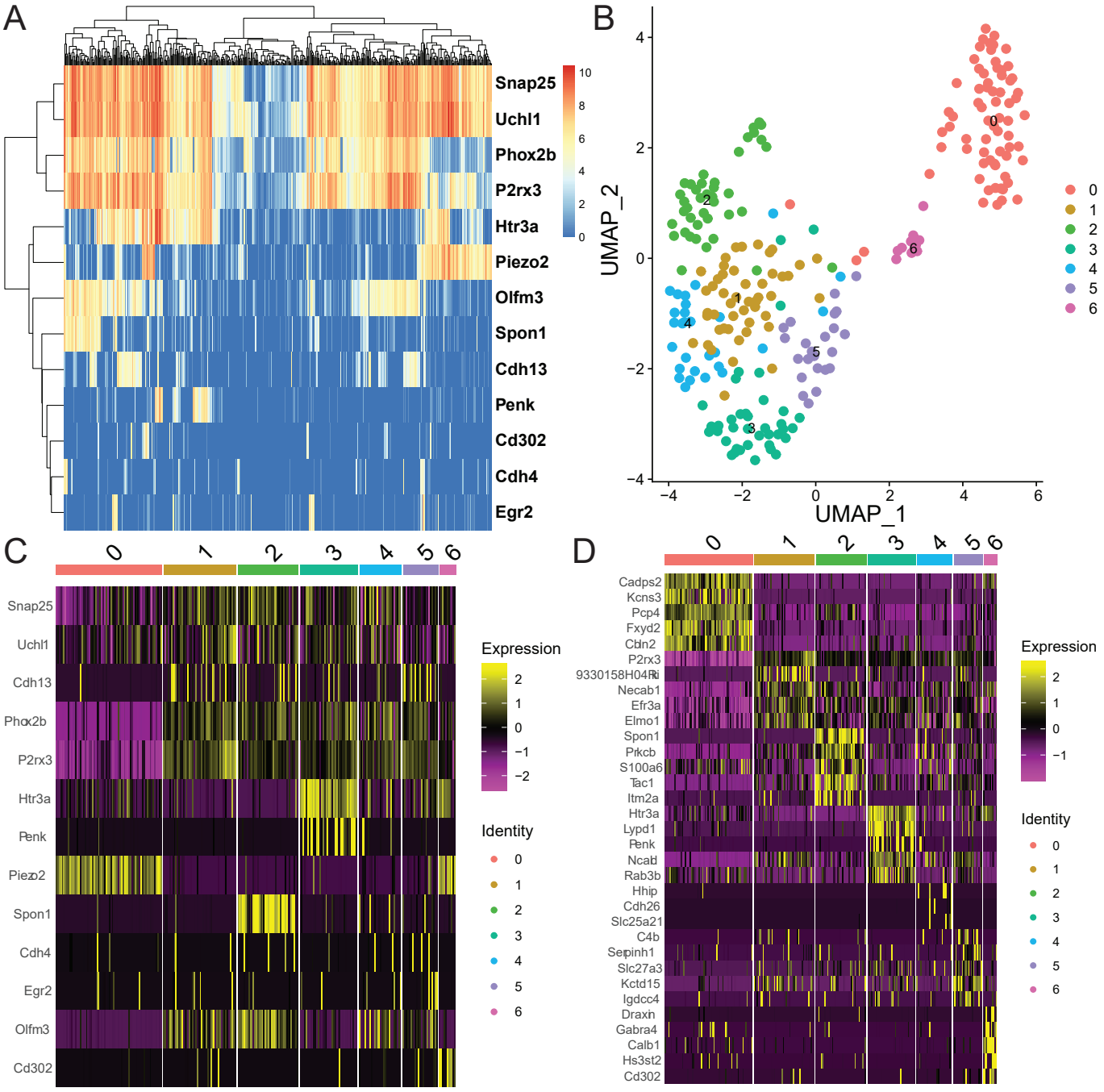
A
Snap25
Uchl1
Phox2b
P2rx3
Htr3a
Piezo2
Olfm3
Spon1
Cdh13
Penk
Cd302
Cdh4
Egr2
10
8
6
4
2
0
B
UMAP_2
UMAP_1
0
1
2
3
4
5
6
C
Expression
Identity
D
Cadps2
Kcns3
Pcp4
Fxyd2
Cbln2
P2rx3
9330158H04Rik
Necab1
Efr3a
Elmo1
Spon1
Prkcb
S100a6
Tac1
Itm2a
Htr3a
Lypd1
Penk
Ncald
Rab3b
Hhip
Cdh26
Slc25a21
C4b
Serpinh1
Slc27a3
Kctd15
Igdcc4
Draxin
Gabra4
Calb1
Hs3st2
Cd302

Figure 4

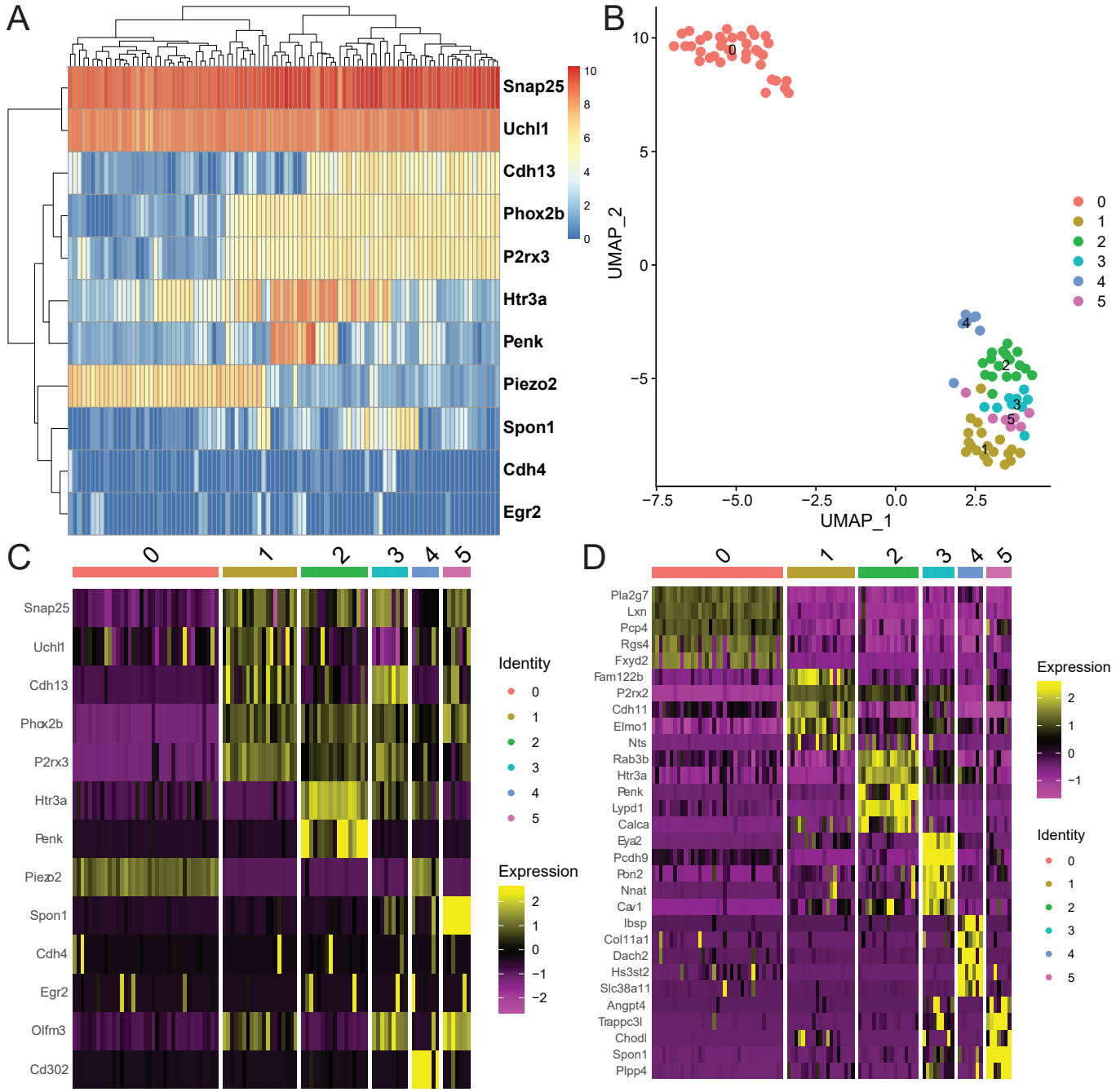
A
Snap25
Uchl1
Cdh13
Phox2b
P2rx3
Htr3a
Penk
Piezo2
Spon1
Cdh4
Egr2
10
8
6
4
2
0
B
UMAP_2
UMAP_1
10
5
0
−5
−7.5
−5.0
−2.5
0.0
2.5
0
1
2
3
4
5
C
0
1
2
3
4
5
Snap25
Uchl1
Cdh13
Phox2b
P2rx3
Htr3a
Penk
Piezo2
Spon1
Cdh4
Egr2
Olfm3
Cd302
Identity
Expression
2
1
0
−1
−2
D
Pla2g7
Lxn
Pcp4
Rgs4
Fxyd2
Fam122b
P2rx2
Cdh11
Elmo1
Nts
Rab3b
Htr3a
Penk
Lypd1
Calca
Eya2
Pcdh9
Pon2
Nnat
Car1
Ibsp
Col11a1
Dach2
Hs3st2
Slc38a11
Angpt4
Trappc3l
Chodl
Spon1
Plpp4
Expression
2
1
0
−1
Identity

Figure 5

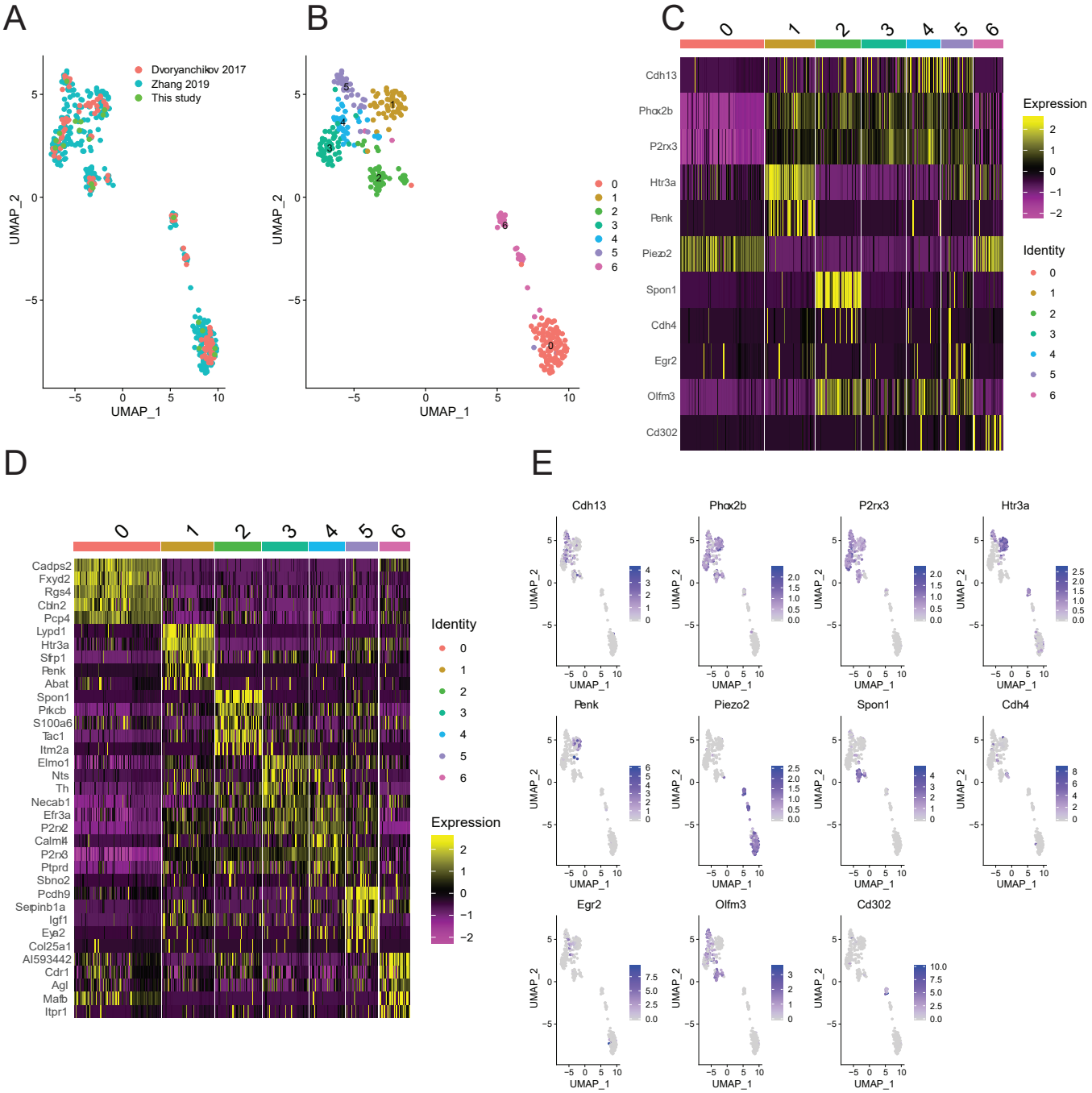
A
Dvoryanchikov 2017
Zhang 2019
This study
UMAP_1
UMAP_2
B
0
1
2
3
4
5
6
C
Cdh13
Phox2b
P2rx3
Htr3a
Penk
Piezo2
Spon1
Cdh4
Egr2
Olfm3
Cd302
Expression
Identity
D
Cadps2
Fxyd2
Rgs4
Cbln2
Pcp4
Lypd1
Htr3a
Sfrp1
Penk
Abat
Spon1
Prkcb
S100a6
Tac1
Itm2a
Elmo1
Nts
Th
Necab1
Efr3a
P2rx2
Calml4
P2rx3
Ptprd
Sbno2
Pcdh9
Serpinb1a
Igf1
Eya2
Col25a1
AI593442
Cdr1
Agl
Maf b
Itpr1
Identity
Expression
E
Cdh13
Phox2b
P2rx3
Htr3a
Penk
Piezo2
Spon1
Cdh4
Egr2
Olfm3
Cd302
UMAP_1
UMAP_2

Figure 6